IOP Conf. Series: Materials Science and Engineering **367** (2018) 012010 doi:10.1088/1757-899X/367/1/012010

Structure Analysis of Fe_3O_4@SiO_2 Core Shells Prepared from Amorphous and Crystalline SiO_2 Particles

Munasir[1,2], A. S. Dewanto[1], D. H. Kusumawati[1,2], N. P. Putri[1,2], A. Yulianingsih[1], I. K. F. Sa'adah[1], A. Taufiq[3], N. Hidayat[3], S. Sunaryono[3], Z. A. I. Supardi[1,2]

[1]Department of Physics, Faculty of Mathematics and Natural Science, Universitas Negeri Surabaya, Jl. Ketintang, Surabaya, 60231, Indonesia
[2]Research Center for Advanced Materials, Universitas Negeri Surabaya, Jl. Ketintang, Surabaya 60231, Indonesia
[3]Department of Physics, Faculty of Mathematics and Natural Science, Universitas Negeri Malang, Jl. Semarang 5, Malang 64145, Indonesia

E-mail: munasir_physics@unesa.ac.id

Abstract: This article reports the results synthesis of crystalline (Fe_3O_4@c-SiO_2) and amorphous (Fe_3O_4@a-SiO_2) nanoparticles from natural resources (iron sand and silica sand). The synthesis of Fe_3O_4 and SiO_2 nanoparticles used co-precipitation and hydrothermal-coprecipitation methods with polyethylene glycol (PEG) 4000 as a template. The XRD data analysis presented that the amorphous SiO_2 particles were successfully produced using hydrothermal and co-precipitation methods. The XRD data analysis also presented that the crystalline phases were formed in quartz and tridymite phases after calcination process of the amorphous phase. SEM images exhibited that the amorphous phase had different particle size and morphology from the crystalline phase. FTIR spectra presented some absorption peaks of new functional groups indicating the existence of Si-O-Si (silanol), Fe-O, C-N, and Fe-O-Si as new functional groups.

Keywords. Core-shell, crystalline and amorphous structures, Fe_3O_4@SiO_2, iron sand, nanoparticle, and silica sand.

1. Introduction

Iron oxide nanoparticle particle has special superior characteristics comparing to other mineral compounds. Naturally, the iron oxide is easily found in iron sand and andesite [1], [2]. The iron oxide has various applications of technologies such as for data saving [3], sensor, spintronic [4], drug delivery system, medical diagnosis [3]–[6], immobilization of protein and enzyme separations [5], [7], [8], and water absorbent [9]–[14]. Related to these applications, particle size strongly determines the electrical, optical, and magnetic properties of the magnetic nanoparticles. Magnetite (Fe_3O_4), besides maghemite (γ-Fe_2O_3) and hematite (α-Fe_2O_3), is an iron oxide that possesses a strong magnetic property. Fe_3O_4 is commonly known as black iron oxide, magnetic iron ore, loadstone, ferrous ferrite, or a Hercules stone that shows the strongest magnetic characteristic [15]–[17].

Despite Fe_3O_4, silica (SiO_2) also has special characteristics that superior to be applied in various applications. In general, the SiO_2 can be found in rocks [1], [18] of about 60 % for example in source

rocks (diorite, gabbro), silica sand, clay or mud, organic material like rice husk ash, and bagasse ash [19]–[21]. The common forms of the SiO_2 crystal structure are quartz, cristobalite, and tridymite [18]. Typically, the SiO_2 nanoparticle has an amorphous phase, and it can be commercially produced as silica gel, fume-silica, and so forth. Several applications of SiO_2 nanoparticles for examples such as medical purposes [22–24], as additives for rubber and plastics [25–27], as fillers for composite construction concrete [28–30], as stabilizers and agents drug delivery and theranostics [23, 31], and as a heavy metal absorbent material in a water filter [14], [22].

In order to increase the application performance of the Fe_3O_4/SiO_2 particles effectively, it is essential to prepare the particles using the inexpensive method from natural resources as raw materials. Based on the previous reports, various methods have been employed such as hydrolysis, microemulsions, and co-precipitation. Meanwhile, the Fe_3O_4/SiO_2 nanocomposites have been fabricated via coprecipitation method [1], [15], [23], [24]. In this work, we exploited a simple co-precipitation method at room temperature which easier to control the particle size of the samples. The main purpose of this research was the synthesis of Fe_3O_4 @ SiO_2 core shells based on natural materials using polyethylene glycol (PEG) 4000 as a template, and analyzing their structure both in amorphous phase (a-SiO_2) and crystalline phase (c-SO_2).

2. Materials and methods

The materials used in this research were silica sand, iron sand, sodium hydroxide (NaOH, 7 M, PA), chloride acid (HCl, 2 M, PA), distilled water, ammonium hydroxide (NH_4OH, 6.5 M, PA), and polyethylene glycol (PEG-4000, PA). The SiO_2 particle formation from silica sand followed equations (1-3), while the fabrication of the Fe_3O_4 particle from iron sand followed equation 4. The preparation process of the SiO_2 particle was initiated by an extraction process to form $Na_2O.xSiO_3$ and $Si(OH)_4$ silica gel with NaCl as a compound of the remaining product.

$$xSiO_{2(s)} + 2NaOH_{(l)} \rightarrow Na_2OxSiO_{3(aq)} + H_2O_{(l)} \quad (1)$$

$$Na_2OxSiO_{3(aq)} + H_2O_{(l)} + 2HCl_{(aq)} \rightarrow Si(OH)_{4(aq)} + 2NaCl_{(aq)} \quad (2)$$

$$Si(OH)_{4(aq)} \ (Drying) \rightarrow SiO_{2(s)} + 2H_2O_{(g)} \quad (3)$$

$$2FeCl_{3(l)} + FeCl_{2(l)} + H_2O_{(l)} + 8NH_4OH_{(l)} \rightarrow Fe_3O_{4(s)} + 8NH_4Cl_{(l)} + 5H_2O_{(l)} \quad (4)$$

The Fe_3O_4 powder from iron sand was reacted with HCl and followed by NH_4OH to form a Fe_3O_4 particle. Furthermore, the preparation of the Fe_3O_4@SiO_2 core shells was conducted using PEG-4000 as a template, and then it will be removed after calcination at (50 to 60) °C. The Fe_3O_4, SiO_2, and PEG were set based on their respective mass composition by comparison of 2:3:3 before draining process at below 60 °C. The crystal structure characterization of the samples was performed using XRD (based on Cu-Kα), while identification of a special functional group of SiO_2 (amorphous and crystalline phases), Fe_3O_4 and Fe_3O_4@SiO_2 employed FTIR. The profile analysis of the samples (morphology and particle size) was done using SEM-EDX.

3. Results and discussion

The diffraction patterns are presented in Figure 1, while the data analysis is presented in Table 1. The figure reveals the existence of a Fe_3O_4 phase with the characteristic peaks (at 2θ): 30.20˚, 35.51˚, 37.23, 43.16˚, 53.51˚, 57.01˚, 62.60˚ and 74.18˚. These peaks are by their respective crystalline indices of (220), (311), (222), (400), (422), (511), (440), and (533) originating from an inverse cubic spinel [17]. In Table 1, the crystal field or peaks (*hkl*) of the experimental sample characteristics are not significantly different from the previous research and shows a similar pattern to the PDF database 00-019-0629 (shown in Table 1). From the results of quantitative analysis using Reitica software with Rietveld method, and modeling referring to suitable the crystallographic database. Moreover, the

sample had a particle diameter of about ~ (25 ± 3.5) nm (d < 100 nm), and was identified as a cubic structure.

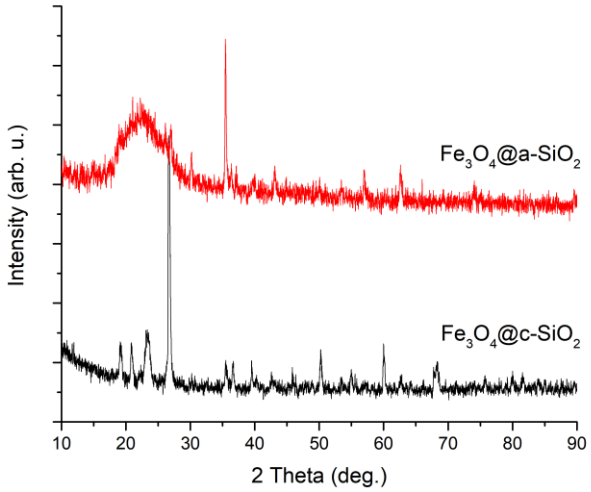

Figure 1. XRD patterns of Fe_3O_4@c-SiO_2 and Fe_3O_4@a-SiO_2 particles: c and a represent the crystalline and amorphous phases.

From Figure 1, it is also found a broad peak at 2θ ≈ 20° to 24° presenting a peak of the amorphous silica. Therefore, the figure proves a combination of the Fe_3O_4 particle and the c-SiO_2 particle. Fe_3O_4 particles that added to the SiO_2 particle as a matrix for crystal or amorphous phase affected the size of the Fe_3O_4@ SiO_2. This phenomenon can be predicted by the growth of finite particles by a large number of Si-O-Si chains on amorphous phase. The diffraction patterns among the Fe_3O_4/c-SiO_2 and Fe_3O_4/a-SiO_2 appears to significantly differ except for a Fe_3O_4 crystal plane identified on the Fe_3O_4/a-SiO_2 diffraction pattern. The results of the phase analysis of the c-SiO_2 sample presented characteristic peaks at 2θ and crystal plane (*hkl*) as shown in Table 1. Hence, the characteristic peaks of the Fe_3O_4/c-SiO_2 composite were identified at 2θ = 30.11˚, 35.54˚, 43.1°, 56.9˚ and 62.5˚ corresponding to their respective crystal plane, i.e. (220), (311), (422), (511), (440).

Table 1. Data analysis of the XRD patterns of the samples

Oxide	*Peak*	*1*	*2*	*3*	*4*	*5*	*6*	*7*	*8*	*9*	*Description*
Fe_3O_4	2θ (deg)	30.07	35.46	43.17	53.55	56.97	62.77				Experimental data
		30.10	35.40	43.10	53.40	56.90	62.60				PDF 00-019-0629
	(hkl)	(220)	(311)	(400)	(422)	(511)	(440)				
SiO_2	2θ (deg)	20.8	26.6	36.5	39.4	45.7	50.1	54.8	59.9	68.1	Experimental data
		20.6	26.6	36.5	39.4	45.7	50.1	54.8	59.9	68.1	PDF 96-901-26101
	(hkl)	(100)	(011)	(110)	(102)	(201)	(112)	(022)	(121)	(203)	

The absorption peaks of the synthesized Fe_3O_4@SiO_2 particles were adjusted to the character peaks of the Fe_3O_4, and SiO_2 resulted from previous research. The analysis was done to identify the functional groups of the samples as shown in Figure 2 and as explained in Table 2. It appears a wavenumber of 543 cm^{-1} that confirmed a vibration on the Fe-O bond, which is a characteristic of the Fe_3O_4. Besides that, the peaks among the Fe_3O_4 and Fe_3O_4@c-SiO_2 or Fe_3O_4@a-SiO_2 particles could also be seen. On the wave number of 1130 cm^{-1} represents the asymmetric vibration of the Si-O-Si and

SiO_2 bonds and a Si-OH bond is found at 900 cm^{-1}. The 3014-3498 cm^{-1} wavenumbers show O-H (water molecule) bond stretching in SiO_2. Such functional groups have similarities with the characteristics of the Fe_3O_4@c-SiO_2 particles obtained from the previous research [25], [26].

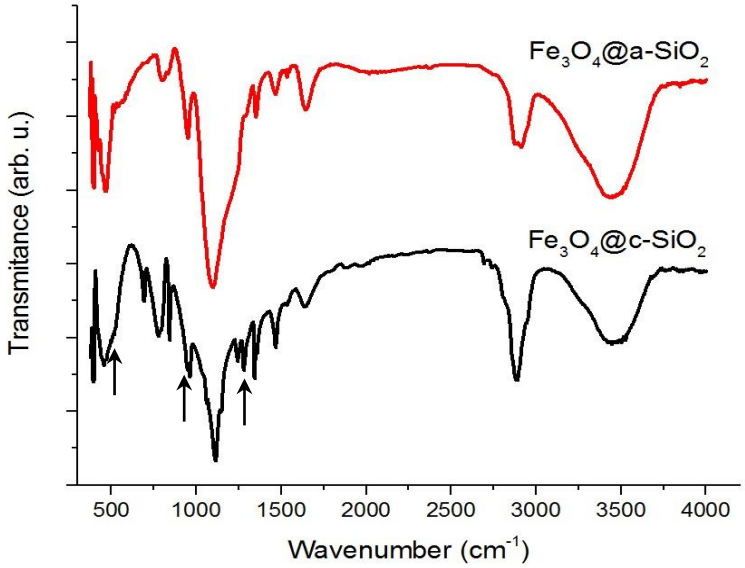

Figure 2. FTIR spectra of Fe_3O_4@c-SiO_2 and Fe_3O_4@a-SiO_2 particles

Table 2. Data analysis results of FITR spectra of the samples

No	*Wave Number (cm^{-1})*	*Functional group*	*Wave Number literature (cm^{-1})*	*Reference*
1	3465	O-H stretching	3650-3200	[27]
2	2870	O-H	1640-3483	[28]
3	1386	Fe-O	1390	[27]
4	1097	Si-O-Si stretching vibration Fe-O-Si stretching	1070-1080	[27], [29]
5	950	Si-O	964	[18], [30]
6	800	Si-O-Si	798	[18], [31]
7	569	Si-O-Fe	570	[1], [32]
8	468	Si-O	461	[18], [31]

According to the results of functional groups adjustment of the Fe_3O_4@a-SiO_2 particles as shown in Table 2, there is a bending vibration on the Si-O bond at the wave number of 468 cm^{-1}. The characteristic peaks between Fe_3O_4 and SiO_2 molecules can be observed as follows: at 569 cm^{-1} and 1097 cm^{-1} wavenumbers identified as stereo types of Fe-O-Si bonds, and wave number 1386 cm^{-1} that identify as the Fe-O group vibration. Thus the process of formation of the Fe_3O_4@SiO_2 composite has successfully produced. At the same time, the presence of Fe-O group indicates Fe_3O_4 particles have an interface bond with the SiO_2 matrix. As shown in Figure 2, there are three arrows showing vibration waves on Fe-O (1386 cm^{-1}) and Fe-O-Si (569 cm^{-1} and 1097 cm^{-1}). On the other hand, the peaks at 468, 800, 950, and 1097 cm^{-1} present asymmetrical vibrations and symmetrical stretching of Si-O-Si siloxane and silanol bonds on silica. Therefore, it indicates that the Fe_3O_4 particles can succeed to form a core formation shell with SiO_2 as a layer [1, 18, 40, 41].The stretching and bending vibration of the H-O-H bond are found at wave numbers of 1641-3465 cm^{-1}. Such functional groups have almost similar characteristics with the Fe_3O_4@a-SiO_2 particles obtained from the references [27], [28].

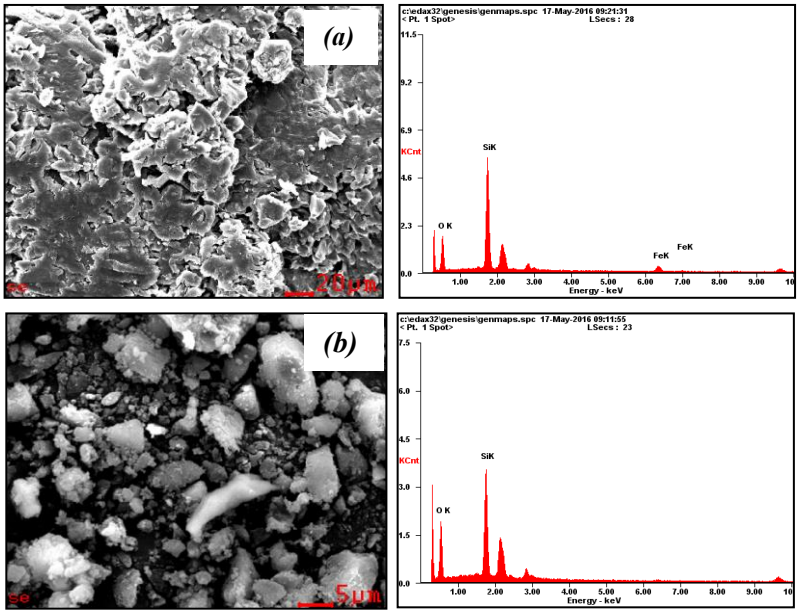

Figure 3. SEM-EDX profiles of Fe_3O_4@SiO_2, with: (a) a-SiO_2 and (b) c- SiO_2 particles

Table 3. Atomic elements of Fe_3O_4@SiO_2 particles

Element	*Fe_3O_4@a-SiO_2*		*Fe_3O_4@c-SiO_2*	
	Wt%	*At%*	*Wt%*	*At%*
O	40.75	57.15	46.15	56.21
Si	47.94	38.30	42.50	39.22
Fe	11.31	04.55	11.35	04.57

Figure 3a Fe_3O_4@a-SiO_2 (for SiO_2 amorphous phase) and Figure 3b Fe_3O_4@ c-SiO_2 (for SiO_2 crystalline phase) are the results of the elective analysis (EDX) for different samples. It appears that the dominant elements of the constituent atom are Si, Fe, and O. The detailed quantitative analysis of the atomic element is presented in Table 3. The elemental atomic content: (i) O Oxygen is 57.15 (At%) and 56.21 (At%); (ii) Si is 38.30 (At%) and 39.22 (At%); (iii) Fe is 4.55 (At%) and 4.57 (At%) respectively. The Fe_3O_4@a-SiO_2 and Fe_3O_4@c-SiO_2 samples show the composition of the constituent elements of the same atom. Morphologically, however, the two samples are different. The Fe_3O_4@ a-SiO_2 sample tends to form amorphous formations as shown in Figure 3a comparing to the crystal formation for Fe_3O_4@c-SiO_2 as shown in Figure 3b. The Fe_3O_4@a-SiO_2 sample tends to form an amorphous phase whereas for Fe_3O_4@c-SiO_2 samples tend to have a crystal phase. Furthermore, Figure 4 represented SEM images with different magnification for all samples show that the crystalline sample has different shape and size of the amorphous sample. The amorphous sample tends to form irregular shape comparing to the crystalline phase. Interestingly, using TEM experiment as shown in Figure 5, the Fe_3O_4@a-SiO_2 sample has successfully produced core-shell structure. Based on the data analysis, it was found that Fe_3O_4 particles presented as core and the a-SiO_2 particles presented shell.

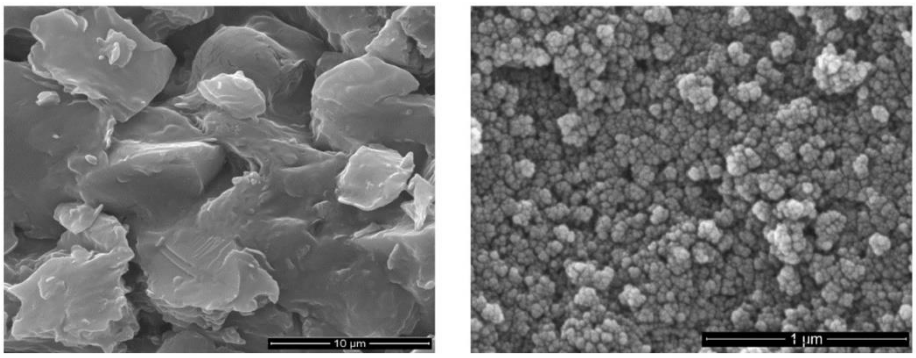

Figure 4. SEM profiles of (a) by a-SiO_2 and (b) c- SiO_2 particles in higher magnification than Figure 3

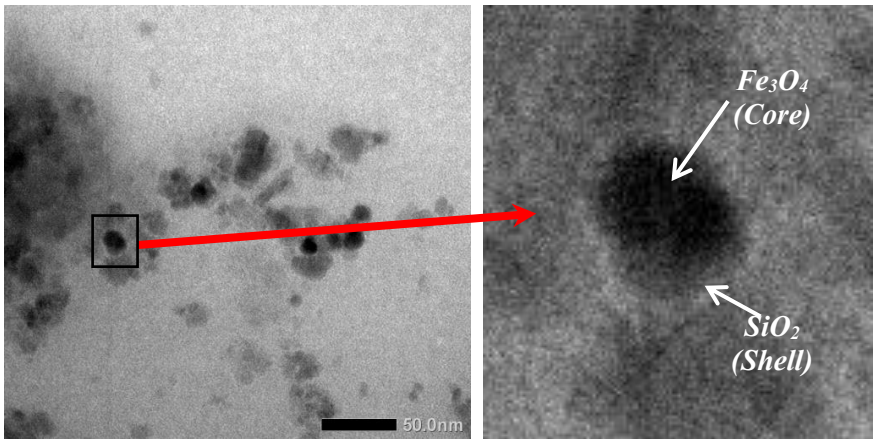

Figure 5. TEM profiles of Fe_3O_4@a-SiO_2 Core-Shell

4. Conclusions

The Fe_3O_4@c-SiO_2 and Fe_3O_4@a-SiO_2 particles have successfully prepared in crystalline and amorphous phases, respectively. The XRD and SEM data analysis showed that the Fe_3O_4 particles had a particle size below 100 nm and served as core covered by SiO_2 particles. The functional groups of the samples exhibited the formation of the SiO_2 and Fe_3O_4 particles.

Acknowledgments

This research was supported by the Ministry of Research, Technology, and Higher Education of Indonesia through the Research Grant.

References

[1] Munasir M *et al* 2017 Composites of Fe_3O_4/SiO_2 from Natural Material Synthesized by Co-Precipitation Method *IOP Conf. Mater. Sci. Eng.* **202** p 012057
[2] Taufiq A *et al* 2015 Nano-Structural Studies on Fe3O4 Particles Dispersing in a Magnetic Fluid Using X-Ray Diffractometry and Small-Angle Neutron Scattering *Mater. Sci. Forum* **827** 213–218
[3] Weller D and Moser A 1999 Thermal Effect Limits in Ultrahigh-Density Magnetic Recording *IEEE Trans. Magn.* **35** 4423–4439
[4] Beg MS *et al* 2017 Porous Fe_3O_4-SiO_2 core-shell nanorods as high-performance MRI contrast agent and drug delivery vehicle *J. Magn. Magn. Mater.* **428** 340–347
[5] Tang L and Cheng J 2013 Nonporous silica nanoparticles for nanomedicine application *Nano Today* **8** 290–312

[6] Lungu I I, Rădulescu M, Mogoşanu G D, and Grumezescu A M 2016 pH sensitive core-shell magnetic nanoparticles for targeted drug delivery in cancer therapy *Rom. J. Morphol. Embryol.* **57** 23–32
[7] Yang S, Zhang X, Zhao W, Sun L, and Luo A 2016 Preparation and evaluation of Fe_3O_4 nanoparticles incorporated molecularly imprinted polymers for protein separation *J. Mater. Sci.* **51** 937–949
[8] Hilczer A, Nowicki M, Czajka R, and Łęska B 2013 Morphology and magnetic properties of Fe_3O_4-alginic acid nanocomposite *Mater. Tehnol.* **1309.7216**
[9] Zhang *Y et al* 2016 Nanomaterials-enabled water and wastewater treatment *NanoImpact.* **3–4** 22–39
[10] Singh S, Barick K C, and Bahadur D 2013 Functional Oxide Nanomaterials and Nanocomposites for the Removal of Heavy Metals and Dyes *Nanomater Nanotechnol* **3** p 20
[11] Olvera R C, Silva S L, Robles-Belmont E, and Lau E Z 2017 Review of nanotechnology value chain for water treatment applications in Mexico *Resour-Effic. Technol.* **3** 1–11
[12] Montero-Campos V and Puente-Urbina A 2016 Continuous-Flow Removal of Arsenic in Drinking Water by Filtering down through Fe_3O_4@SiO_2 Magnetic Composite *J. Water Resour. Prot.* **08** 619–630
[13] Tiwari D K, Behari J, and Sen P 2018 Application of Nanoparticles in Waste Water Treatment *World Appl. Sci. J.* **3** 417–433
[14] Ahmaruzzaman M and Gupta V K 2011 Rice Husk and Its Ash as Low-Cost Adsorbents in Water and Wastewater Treatment *Ind. Eng. Chem. Res.* **50** 13589–13613
[15] Sonmez M *et al* 2015 Synthesis and Applications Of Fe3O4/SiO2 Core-Shell Materials *Curr. Pharm. Des.* **21** 5324–5335
[16] Bahtiar S *et al* 2017 Synthesis Investigation on Structural and Magnetic Behaviors of Spinel M-Ferrite [M = Fe; Zn; Mn] Nanoparticles from Iron Sand *IOP Conf. Ser. Mater. Sci. Eng.* **202** p 012052
[17] Abbas M, Takahashi M, and Kim C 2013 Facile sonochemical synthesis of high-moment magnetite Fe_3O_4 nanocube *J. Nanoparticle Res.* **15**
[18] Munasir, Triwikantoro, Zainuri M, and Darminto 2015 Synthesis of SiO_2 nanopowders containing quartz and cristobalite phases from silica sands *Mater. Sci-Pol.* **33** 47–55
[19] Affandi S *et al* 2009 A facile method for production of high-purity silica xerogels from bagasse ash *Adv. Powder Technol.* **20** 468–472
[20] Nittaya A N and Thuadaij 2008 Preparation of Nanosilica Powder from Rice Husk Ash by Precipitation Method *Chiang. Mai. J. Sci* .**35** 206–211
[21] Trabelsi W Benzina M and Bouaziz S 2009Physico-chemical characterisation of the Douiret sand Southern Tunisia: Valorisation for the production of Silica Gel *Phys. Procedia* **2** 1461–1467
[22] Barbé C *et al* 2013 Silica Particles: A Novel Drug-Delivery System *Adv. Mater.* **16** 1959–1966
[23] Kwon S *et al* 2013 Silica-based mesoporous nanoparticles for controlled drug delivery *J Tissue Eng* **4** p 2041731413503357
[24] Karimi Pasandideh E *et al* 2016 Silica-coated magnetite nanoparticles core-shell spheres Fe_3O_4@SiO_2 for natural organic matter removal *J. Environ. Health. Sci. Eng.* **14** p 21
[25] Conradi M 2013 Nanosilica-Reinforced Polymer Composite *Mater. Technol.* **47** 285–293
[26] Marquis D M, Guillaume É, and Chivas-Joly C 2011 Properties of Nanofillers in Polymer *Nanocomposites. Polym. Anal. Methods.* **InTech**
[27] Chen Y *et al* 2008 Natural rubber nanocomposite reinforced with nano silica *Polym. Eng. Sci.* **48** 1674–1677
[28] Said AM Zeidan MS Bassuoni MT and Tian Y 2012 Properties of concrete incorporating nano-silica *Constr. Build Mater.* **36** 838–844
[29] Park J T, Lee K J, Kang M-S, Kang Y S, and Kim J H 2007 Nanocomposite polymer

electrolytes containing silica nanoparticles: Comparison between polyethylene glycol and polyethylene oxide dimethyl ether *J. Appl. Polym. Sci.* **106** 4083–4090
[30] Mizutani T, Arai K, Miyamoto M, and Kimura Y 2006 Application of silica-containing nano-composite emulsion to wall paint: A new environmentally safe paint of high performance *Prog. Org. Coat.* **55** 276–283
[31] Luo Z, Xu Y, and Ye Q 2015 Effect of nano-SiO_2-LDPE packaging on biochemical sensory and microbiological quality of Pacific white shrimp Penaeus vannamei during chilled storage *Fish Sci.* **81** 983–993
[32] Anjum M, Miandad R, Waqas M, Gehany F, and Barakat M A 2016 Remediation of wastewater using various nano-materials *Arab. J. Chem.*
[33] Peternele W S *et al* 2014 Experimental Investigation of the Coprecipitation Method: An Approach to Obtain Magnetite and Maghemite Nanoparticles with Improved Properties *J. Nanomater* **2014** 1–10
[34] Majeed J, Ramkumar J, Chandramouleeswaran S, and Tyagi A K 2014 Fe_3O_4@SiO_2 core-shell nanoparticles: Synthesis characterization and application in environmental remediation *AIP Conference Proceedings* **1591** pp 605–607
[35] Bini R A *et al* 2012 Synthesis and functionalization of magnetite nanoparticles with different amino-functional alkoxysilanes *J. Magn. Magn. Mater.* **324** 534–539
[36] Silva V A J *et al* 2013 Synthesis and characterization of Fe_3O_4 nanoparticles coated with fucan polysaccharides *J. Magn. Magn. Mater.* **343** 138–143
[37] Quy D V *et al* 2013 Synthesis of Silica-Coated Magnetic Nanoparticles and Application in the Detection of Pathogenic Viruses *J. Nanomater* **2013** 1–6
[38] Munasir, Sulton A, Triwikantoro, Zainuri M, and Darminto 2013 Synthesis of silica nanopowder produced from Indonesian natural sand via alkalifussion route *AIP. Conf. Proc. AIP Publishing* **1555** pp 28–31
[39] Hui C *et al* 2011 Core-shell Fe_3O_4@SiO_2 nanoparticles synthesized with well-dispersed hydrophilic Fe3O4 *Nanoscale* **3** 701–705
[40] Alizadeh A *et al* 2012 Biguanide-Functionalized Fe_3O_4/SiO_2 Magnetic Nanoparticles: An Efficient Heterogeneous Organosuperbase Catalyst for Various Organic Transformations in Aqueous Media Bull *Korean Chem. Soc.* **33** 2546–2552
[41] Jal P K, Sudarshan M, Saha A, Patel S, and Mishra B K 2004 Synthesis and characterization of nanosilica prepared by precipitation method *Colloids Surf. Physicochem. Eng. Asp.* **240** 173–178
[42] Ahangaran F, Hassanzadeh A, and Nouri S 2013 Surface modification of Fe_3O_4@SiO_2 microsphere by silane coupling agent *Int. Nano. Lett.* **3** p 23
[43] Hui C *et al* 2011 Core-shell Fe_3O_4@SiO_2 nanoparticles synthesized with well-dispersed hydrophilic Fe3O4 seeds *Nanoscale* **3** 701–705